

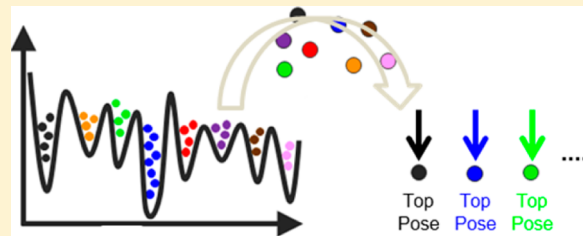
# Ensemble-Based Docking Using Biased Molecular Dynamics

Arthur J. Campbell, Michelle L. Lamb, and Diane Joseph-McCarthy\*,†

AstraZeneca, R&D Boston, 35 Gatehouse Drive, Waltham, Massachusetts 02451, United States

## Supporting Information

**ABSTRACT:** Proteins are dynamic molecules, and understanding their movements, especially as they relate to molecular recognition and protein–ligand interactions, poses a significant challenge to structure-based drug discovery. In most instances, protein flexibility is underrepresented in computer-aided drug design due to uncertainties on how it should be accurately modeled as well as the computational cost associated with attempting to incorporate flexibility in the calculations. One approach that aims to address these issues is ensemble-based docking. With this technique, ligands are docked to an ensemble of rigid protein conformations. Molecular dynamics (MD) simulations can be used to generate the ensemble of protein conformations for the subsequent docking. Here we present a novel approach that uses biased-MD simulations to generate the docking ensemble. The MD simulations are biased toward an initial protein–ligand X-ray complex structure. The biasing maintains some of the original crystallographic pocket-ligand information and thereby enhances sampling of the more relevant conformational space of the protein. Resulting trajectories are clustered to select a representative set of protein conformations, and ligands are docked to that reduced set of conformations. Cross-docking to this ensemble and then selecting the lowest scoring pose enables reliable identification of the correct binding mode. Various levels of biasing are investigated, and the method is validated for cyclin-dependent kinase 2 and factor Xa.



## INTRODUCTION

A successful drug discovery program often requires an extensive commitment of time and financial resources; 10–15 years and over a billion dollars are generally necessary to bring a drug from inception to market.<sup>1</sup> Predictive techniques aimed at reducing the cost of drug discovery are highly valued and are being actively applied and further developed. Computational chemistry approaches for drug design are among the most mature and predictive, and yet areas for improvement remain. Computational chemists use a wide variety of approaches to aid in effective and efficient lead generation, identification, and optimization, with the ultimate goal of shortening project timelines and delivering high-quality candidate drugs. In the area of structure-based design, for example, challenges remain with the accurate incorporation of protein flexibility, solvation, and ligand electronic effects. In this manuscript, we address the issues associated with including protein flexibility in docking. A novel ensemble-based docking approach using biased molecular dynamics (MD) simulations is presented and validated.

In structure-based drug design, three-dimensional (3D) structural information about the target macromolecule is utilized in the design of potent and selective inhibitors of the target. Once a lead is identified, potentially through structure-based virtual screening, a multivariate optimization process ensues. Often an X-ray structure of the target with a lead molecule bound is obtained. Proposed modifications to the lead molecule, including libraries of possible ligands, are docked into the target binding site. Compounds are selected for synthesis based on their predicted binding mode and predicted binding affinity as well as synthetic accessibility. If there are physical

property or selectivity concerns about the initial lead, compounds may be selected for synthesis which are expected to maintain and not necessarily improve the potency but modulate another property or affinity for a secondary target. While in the ideal situation target–ligand complex structures are obtained for subsequently synthesized, assayed, and improved ligands, it is not uncommon for a project to have limited structural information, such as one or a few target–ligand complex structures (possibly only a target-substrate structure) or only an apo structure.

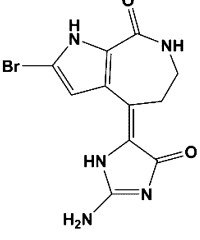
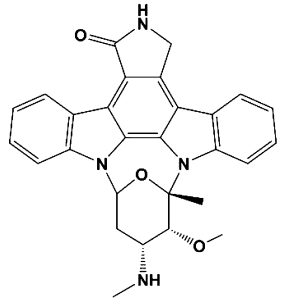
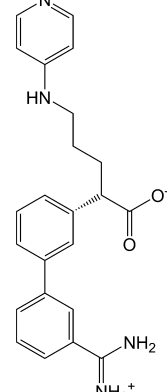
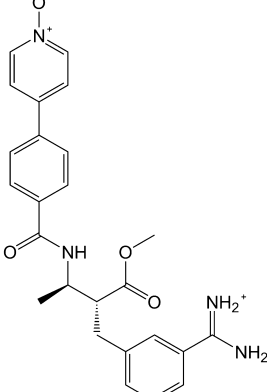
When a ligand binds to a target protein it may induce a specific pocket conformation. If an X-ray structure of the protein–ligand complex exists, the ligand may be modified or optimized to bind to the pocket conformation that is captured in the X-ray complex structure. It is likely that this pocket conformation is not the only biologically relevant conformation. Most commonly used docking programs, however, keep the protein molecule fixed and flexibly dock the ligand. Techniques that account for some degree of protein flexibility should be expected to increase the docking accuracy, both in terms of binding mode and affinity prediction. Attempts at including macromolecular motion, however, have sometimes resulted in the introduction of noise into the calculations and generation of potentially irrelevant pocket conformations, leading to decreased docking accuracy.<sup>2</sup>

Protein flexibility can be accounted for in docking through direct simulation of the target–ligand complex or by docking to

Received: December 9, 2013



Table 1. Chemical Structures of CDK2 (left) and FXa (right) Ligands

System	CDK2		FXa	
PDB	1DM2	1AQ1	1XKA	1KSN
Ligand Name	Hymenialdisine	Staurosporine	FX-2212A	FXV673
Ligand Structure				
Ligand Abbrev.	CDK2:L1	CDK2:L2	FXa:L1	FXa:L2
Protein Abbrev.	CDK2:P1	CDK2:P2	FXa:P1	FXa:P2
Complex Abbrev.	CDK2:P1-L1	CDK2:P2-L2	FXa:P1-L1	FXa:P2-L2

an ensemble of rigid protein conformations. Simulation-based approaches include both MD<sup>3,4</sup> and Monte Carlo (including rapid torsional Monte Carlo simulations as implemented in QXP).<sup>5</sup> MD simulations are not used routinely in drug design due to the time required to setup and analyze the results as well as the computational time required for a production run for each proposed ligand. Advances in the development of force fields (e.g., Amber FF99SB)<sup>6</sup> and parallelization of MD code<sup>7–9</sup> are beginning to make these calculations more practical, but they are still relatively long on the time scale of a drug design optimization cycle. Recently, it has been shown that long time-scale simulations, using highly parallel code on hardware specialized for MD,<sup>10</sup> can recapitulate binding modes of individual ligands if docked within the vicinity of the binding pocket.<sup>11</sup> In addition, visualization of a simulation may in certain instances provide insight into the mechanism of the target and/or help to explain why certain ligands may preferentially bind to the target.

A number of ensemble-based docking techniques have also been developed and explored.<sup>12,13</sup> Ensembles of protein conformations can be generated from a set of existing 3D X-ray structures or an NMR structure (e.g., refs 14–16), through homology modeling (e.g., induced fit docking (IFD))<sup>17</sup> or through simulation (e.g., the relaxed complex scheme,<sup>18,19</sup> IFREDA,<sup>20</sup> or dynamic pharmacophore model<sup>21</sup>). The use of multiple crystal structures for ensemble docking may, of course, be biased by the structures that are available, especially if all the ligands bound are close analogues. In addition, information obtained from NMR experiments has been utilized in general as MD restraints<sup>22</sup> and in particular to generate conformational ensembles for docking.<sup>23,24</sup> While promising, these methods require that such NMR data be readily available. With IFD, alanine mutations and softened docking potentials are employed to enhance sampling of binding modes. IFD is

currently limited to the movements of side chains and certain specified stretches of the backbone. Normal mode analysis has also been exploited for ensemble docking with some success,<sup>25–27</sup> but has not been routinely adopted by pharmaceutical computational chemists either, perhaps due to ease of use and time restrictions.

In this manuscript, we present a novel ensemble-based docking approach using biased-MD simulations to generate the ensemble. Starting with a protein–ligand complex structure, an MD simulation is run at room temperature with a biasing potential applied to the ligand. During the simulation, which is used to generate the ensemble of protein conformations, a biasing potential is utilized to restrict the sampling of the pocket conformation. Only pocket conformations relatively close to those of the existing liganded structure are sampled to reduce the noise introduced into the subsequent docking calculations, while still allowing a significant degree of side chain and backbone flexibility. Various ligand restraints are explored and the accuracy and reproducibility of the overall approach is assessed.

## METHODS

**Test cases.** Two test systems, cyclin-dependent kinase 2 (CDK2) and factor Xa (FXa), are used to develop and validate the ensemble docking via biased-MD approach. For each protein, two liganded structures were selected and prepared. Each pair of structures was selected such that cross-docking of at least one of the ligands into the other protein structure failed. For each protein system, to allow for a direct comparison of the MD simulations starting with a given complex structures, respectively, the proteins were prepared such that they were chemically equivalent, as described below.

CDK2 is a serine/threonine protein kinase involved in the regulation of the cell cycle; inhibition of CDK2 is known to

arrest the cell cycle and as such small-molecule inhibitors of CDK2 can block the overproliferation of cancerous cells. When ATP binds to CDK2, as with other kinases, the adenine ring forms two hydrogen bonds with the backbone hinge-region (Glu-81 and Leu-83).<sup>28</sup> A CDK2-hymenialdisine (1DM2.pdb) and a CDK2-staurosporine (1AQ1.pdb) complex structure were selected and will be referred to herein as CDK2:P1-L1 and CDK2:P2-L2, respectively. The CDK2:P1-L1 structure contained four ethylene glycol molecules which were removed.

FXa is a serine protease which is involved in the blood coagulation cascade.<sup>29</sup> Inhibitors of FXa have been found to be useful as anticoagulants.<sup>30</sup> The active site of FXa is a solvent-exposed shallow pocket, as opposed to CDK2 which contains a deep hydrophobic active site. For this target, FXa-FX-2212a (1XKA.pdb)<sup>31</sup> and FXa-FXV673 (1KSN.pdb)<sup>32</sup> complex structures were selected and will be referred to as FXa:P1-L1 and FXa:P2-L2, respectively. The ligand FX-2212A is (2S)-(3'-amidino-3-biphenyl)-5-(4-pyridylamino) pentanoic acid, and FXV673 refers to 2-(R)-(3-carbamimidoylbenzyl)-3-(R)-[4-(1-oxypyridin-4-yl)benzoylamino]-butyric acid methyl ester. FXa is a dimer that consists of two chains, the light chain (L) and the heavy chain (H). The light chain is composed of the Gla domain (L:41–85) and epidermal growth factor (EGF)-like domains, EGF1 (L:86–122) and EGF2 (L:125–165). The heavy chain contains the catalytic domain (H:235–488). See Table 1 for a summary of these test cases.

**Preparation of Systems for MD.** For both CDK2 and FXa, the MOE software package (Chemical Computing Group, 2011, Montreal, Quebec) was used to visualize and select the protein system for MD (see the fully prepared systems in Figure 1). To allow simulation of the full system and to ensure

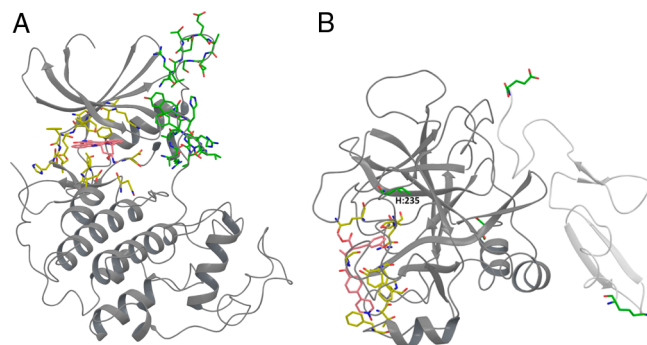


**Figure 1.** Fully prepared MD protein systems are shown in (A) for CDK2 (derived from 1AQ1.pdb) and in (B) for FXa (derived from 1KSN.pdb). The protein backbone is shown in a gray ribbon diagram. Residues shown in sticks colored by element include the binding site residues with carbons in yellow, the ligand with carbons in pink, and the model built regions with carbons in green. For FXa, the light chain is depicted by the lighter gray ribbon diagram.

that the prepared protein structures are chemically equivalent, for CDK2 regions disordered in the X-ray structures were model built, using the fully ordered CDK2 kinase structure, 1YKR.pdb,<sup>33</sup> as a template. These disordered regions, all outside of the ligand binding pocket, are residues 36–44 and 149–163 in CDK2:P1-L1 and residues 36–43 and 149–161 in CDK2:P2-L2. Ordered waters were included if within 10 Å of the retained protein structure. Each complete CDK2 system was then protonated using Protonate 3D in MOE. Termini were charged. Due to obvious steric clashes in CDK2:P1-L1 for residues 148–149 and 163–164, atoms in these residues were

minimized using the GizMOE minimizer in MOE, using the default settings (MMFF94X force field and a root-mean-square deviation (RMSD) gradient of 0.05 kcal/mol·Å).

For FXa, regions of the protein structure which were disordered in either one of the two complexes were removed. The ordered residues in the X-ray structures are L:89–179 and H:235–469 for FXa:P1 and L:127–178 and H:235–468 for FXa:P2. Therefore, the remaining chemically equivalent systems used for dynamics for FXa consist of L:127–178 and H:235–468. Ordered waters were included if within 10 Å of the retained protein structure. A calcium ion present in both structures, and located ~25 Å outside the ligand binding pocket, was also retained. For the FXa systems, the protein was protonated, missing atoms at chain termini were built, and cysteine disulfide bonds formed (L:129–L:140, L:136–L:149, L:151–L:164, L:172–H:342, H:241–H:246, H:261–H:277, H:390–H:404, and H:415–H:443) using the Leap module of Amber 11<sup>7</sup> with the ff99SB force field.<sup>6</sup>

For both CDK2 and FXa proteins, parameters (atom types and partial charges) were assigned using Leap with the ff99SB force field.<sup>6</sup> For each ligand (Table 1), AM1-BCC<sup>34,35</sup> partial charges were generated using the Antechamber module in Amber. Leap was used with the GAFF potential<sup>36</sup> to generate the additional force field parameters for each ligand. For MD simulations performed using the “double impropers MD” protocol described below, the resulting force constants for improper dihedrals were doubled to restrict the planarity of the ligand. The specific ligand parameters used are given in Tables S1–S4. Modified Ca<sup>2+</sup> parameters were taken from Bradbrook et al.<sup>37</sup> Each complex system (including ordered waters) was then solvated with TIP3P water molecules<sup>38</sup> using a truncated octahedron periodic box with an 8 Å buffer, resulting in a total of 8298 (CDK2:P1-L1), 9378 (CDK2:P2-L2), 8088 (FXa:P1-L1), and 7594 (FXa:P2-L2) water molecules, respectively. The difference in the number of waters for “equivalent systems” is due to the variation in ordered waters associated with each structure; the CDK2:P2-L2 system, for example, has 40 more ordered waters than the CDK2:P1-L1 system, resulting in a slightly larger and slightly differently placed periodic box. For all simulations, the long-range electrostatics are calculated using the particle mesh Ewald method<sup>39,40</sup> with a nonbonded cutoff of 8 Å.

**General MD Workflow.** All MD simulations carried out for this approach consist of two stages of minimization and equilibration dynamics prior to a production run (Figure 2). Minimization is carried out at constant volume and consists of a total of 10,000 steps, 10 steps of steepest descent, followed by 9990 steps of conjugate gradient. Equilibration involves dynamics performed, in three consecutive sets, with a time step of 1 fs and using SHAKE to constrain bonds involving hydrogen.<sup>41</sup> Production dynamics consists of 5 ns of dynamics carried out under constant pressure (1 atm, maintained using a pressure relaxation time of 1.0 ps) and temperature (298 K, maintained via a weak coupling algorithm with a coupling constant of 1.0 ps). A time step of 2 fs is employed with SHAKE. See Figure 2 and the text below for a more detailed description of the parameters used during each stage of the simulation.

During Stage I of minimization and equilibration, for the minimization heavy atoms in the protein, ligand, and ordered waters are restrained, using a force constant of 100.0 kcal/mol·Å<sup>2</sup>. The same restraints are applied during the first 100 ps of equilibration, except that atoms which were model-built into

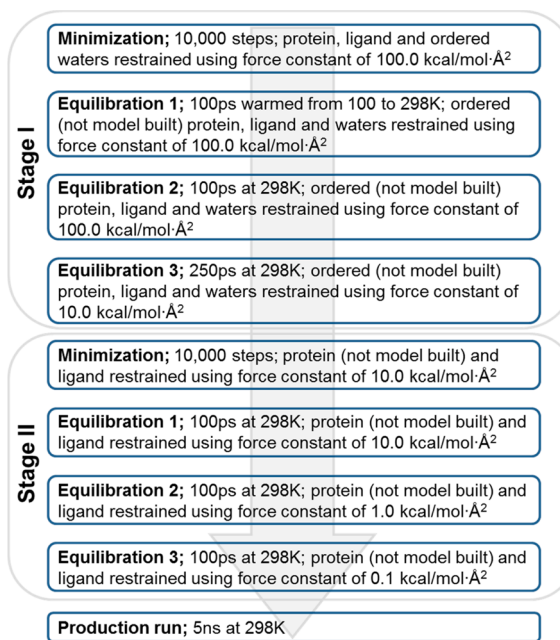


Figure 2. General MD workflow.

the system are now unrestrained. During this equilibration (Equilibration 1), the system is gradually heated from 100 to 298 K at constant volume. Two additional sets of equilibration at constant pressure (1 atm, with a pressure relaxation time of 0.1 ps for the first set and 0.5 ps for the second set) and temperature (298 K, with a coupling constant of 0.1 ps for the first set and 0.5 ps for the second set) follow, for a total 450 ps of dynamics. Equilibration 2 is performed for 100 ps with the restraints described above, and Equilibration 3 is carried out for 250 ps with the restraint force constant reduced to 10.0 kcal/mol·Å<sup>2</sup>.

During Stage II of minimization and equilibration, for the minimization, protein backbone atoms (except for those that were model built) and heavy atoms of the ligand are restrained using a force constant of 10.0 kcal/mol·Å<sup>2</sup>. Three consecutive sets of 100 ps equilibration dynamics follow, with decreasing restraint force constants of 10.0, 1.0, and 0.1 kcal/mol·Å<sup>2</sup>, respectively, for a total of 300 ps. This equilibration dynamics was carried out at constant pressure (1 atm, with a pressure relaxation time of 0.5 ps) and temperature (298 K, with a coupling constant of 0.5 ps).

For the production dynamics, all atoms are unrestrained with the “normal MD” and “double impropers MD” protocols, while with the “restrained MD” protocol heavy atoms of the ligand are restrained using a force constant of 0.1 kcal/mol·Å<sup>2</sup>.

**MD Production Protocols Investigated.** For each protein system, three MD protocols are investigated: (i) “normal MD”, (ii) “restrained MD” with the ligand position restrained, and (iii) “double impropers MD” with the force constants on all ligand improper dihedral angles doubled (see Tables S1–S4). These three MD protocols vary the restraints applied to the ligand, to investigate their effect on the sampling of the protein conformation, and consequently the quality of the ensemble of representative structures generated with respect to docking accuracy. For each protein–ligand system and MD protocol explored, five independent MD simulations are run using different initial velocities to verify the reproducibility of the approach.

**Generating an Ensemble of Representative Structures.** An ensemble of representative structures for docking is generated from each MD simulation. The objective is to create a reduced set of protein conformations from each MD trajectory, such that the conformations most relevant for ligand binding are represented. It is not generally practical to dock to the thousands of snapshots of the protein generated by an MD simulation, and in fact doing so may introduce irrelevant conformations that could reduce the docking accuracy. A carefully selected ensemble should improve the docking results by incorporating some degree of protein flexibility in a relative quick time frame.

For a given MD simulation, protein conformations (at each ps) are clustered using the mass-weighted average-linkage RMSD-based cluster algorithm,<sup>42</sup> as implemented in the ptraj module of Amber. Cheatham and co-workers showed average linkage to be one of the best performing clustering methods, especially when the cluster number is given in advance. The target number of clusters was set to eight to select eight representative protein pocket conformations from each MD simulation as the docking ensemble. Initial calculations docking to ensembles with six representative structures, instead of eight, yielded results with slightly lower accuracy (data not shown). In studies using multiple X-ray structures to generate ensembles for docking, including 3–5 structures per ensemble has produced reasonable results.<sup>15,43</sup> With ensembles based on MD snapshots, compared to protein X-ray structures, it is possible to include more conformations, and it may be desirable since these are simulated and not experimental conformations. The most representative protein pocket conformation from each cluster, the snapshot closest to the cluster centroid, is selected for inclusion in the docking ensemble. The residues are selected to define the binding pocket, and the distance to the cluster centroid is determined based on the RMSD of all atoms of the selected residues, to focus on clusters in the appropriate local region of the protein structure. The binding pocket is defined for CDK2 by residues 10, 18, 31, 33, 64, 80–84, 86, 131, 134 and 145, and for FXa by residues H:318–319, H:396, H:413–414, H:416, H:419, H:439–440 and H:442. As an example of the resulting conformational variation within an ensemble, in one CDK2 ensemble the pairwise heavy atom RMSD for all binding site residues ranged from 0.63 to 0.84 Å and for side chain atoms only ranged from 0.76 to 1.05 Å, with the largest side chain RMSD at 2.6 Å. Similarly, in one FXa ensemble the pairwise heavy atom RMSD for all binding site residues ranged from 0.70 to 1.06 Å and for side chain atoms only ranged from 0.86 to 1.33 Å, with the largest side chain RMSD at 2.4 Å.

**Preparation of Ensemble Conformations for Docking.** After generating an ensemble, each of the eight protein conformations in the ensemble is prepared for docking using Maestro version 9.2 (Schrodinger, LLC, 2011, New York, NY). Solvent is removed, the protein conformation is aligned to its respective X-ray complex structure using the Protein Structure Alignment module, and hydrogen positions are regenerated using Epik version 2.2 from Protein Preparation Wizard. Reprotonating the complex in this manner, to ensure that the hydrogen positions were placed using the same force field employed for the docking, yielded slightly better results than keeping the original hydrogen positions from the MD (data not shown).

**Docking Calculations.** Glide version 5.7 is employed with Glide SP scoring<sup>44,45</sup> for all docking calculations. Docking grids

are generated using the default settings where the position of the ligand (either from the minimized X-ray structure in the case of direct docking or from the MD simulation in the case of ensemble docking) is selected to define the center of the receptor site. Ligand conformations are prepared for docking starting from the X-ray conformations and using LigPrep version 2.5 with the ionizer and pH set to  $7.0 \pm 1.0$  and chiralities determined from the input structure and defaults for other settings.

**Analysis of Docking Results.** Following docking, the RMSD for heavy atoms of the docked ligand pose from its corresponding X-ray position is calculated using the Maestro superposition function. A correct or near native pose is defined as a docking pose with an RMSD of  $\leq 2$  Å from its corresponding X-ray position. For the ensemble docking, the best docking pose is selected from the eight ligand poses generated from the ensemble based on the Glide SP docking score. Then, the docking accuracy is assessed with respect to that binding mode prediction using the RMSD measure.

**Preparation of X-ray Structures for Direct Docking.** For CDK2 and FXa, respectively, the starting complex structures (Table 1), taken directly from the Protein Data Bank (<http://www.rcsb.org>), were aligned using Protein Structure Alignment and prepared using the Protein Preparation Wizard in Maestro version 9.2 (Schrodinger, LLC, 2011, New York, NY). Hydrogens were added, all waters and ions were removed, hydrogens were minimized, and then the entire structure was minimized with constraints using default settings.

## RESULTS AND DISCUSSION

In this work, a novel ensemble-docking via biased-MD approach (Figure 3) is developed and validated using CDK2 and FXa as test systems. CDK2 and FXa were selected because their binding pockets are substantially different in character; the ATP binding site in CDK2 is a deep hydrophobic pocket, while the FXa binding pocket is relatively shallow and solvent exposed (Figure 4). The specific complex structures chosen as test cases for each system (i.e., CDK2 and FXa) were selected

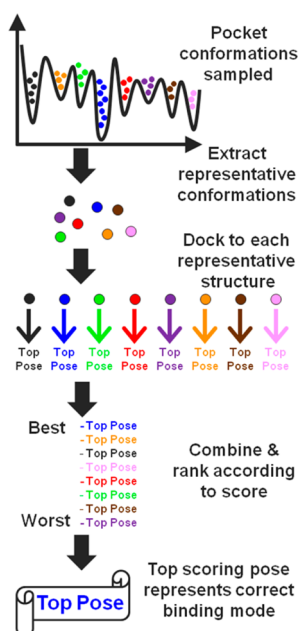


Figure 3. Ensemble docking via biased-MD workflow.

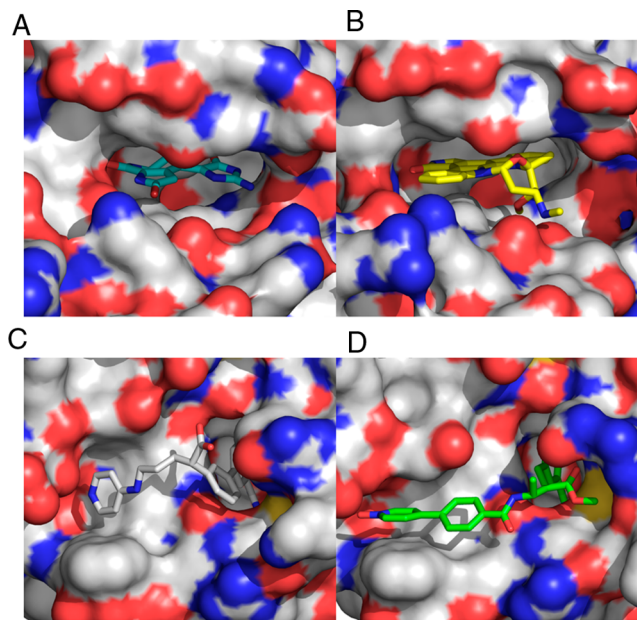
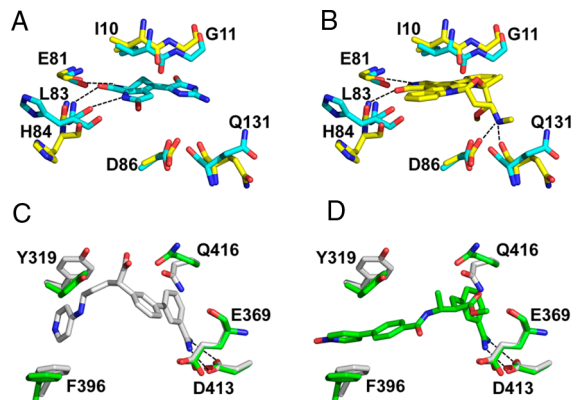


Figure 4. X-ray structures of (A) CDK2:P1-L1 (1DM2.pdb), (B) CDK2:P2-L2 (1AQ1.pdb), (C) FXa:P1-L1 (1XKA.pdb), and (D) FXa:P2-L2 (1KSN.pdb) complexes are shown with a molecular surface on the protein colored by atom type and with the bound ligand in thick sticks colored by element. For each protein system, the structures are shown in the same frame of reference. Figures were generated using PyMOL (The PyMOL Molecular Graphics System, version 1.5.0.4 Schrödinger, LLC).

because cross-docking to the rigid protein was expected to fail, in at least one case, based on published results using IFD without alanine mutations.<sup>17</sup> In addition, the corresponding pairs of ligands are chemically diverse. The test cases probe our ability to predict the correct binding mode if only one of the two protein structures were known. While the two CDK2 ligands are substantially different in size and chemical composition, they make similar hydrogen bonds to the hinge region (Glu-81, Leu-83) in the binding pocket (Figure 5A and B). The two FXa complex ligands make interactions between the amino groups of each ligand and the carboxyl group of Asp 413 (Figure 5C and D), and both have a large number of rotatable bonds (9 and 10, respectively), making them difficult docking test cases in general. These systems have also been widely studied computationally.<sup>17,46</sup>

To show that the selected test cases are in fact relevant for this study, for both systems, the ligands were first docked to each of the two rigid protein structures (Table 2). We chose to use the Glide docking program<sup>44,45</sup> because it is widely used in the pharmaceutical industry due to its overall accuracy across a wide range of target classes and its general ease of use and reliability.<sup>47–49</sup> While there are many other docking programs that we could have employed (see refs 50 and 51 for examples), our purpose was to show that docking to ensembles generated by biased-MD could improve upon the results that are possible with a standard docking program. Our biased-MD approach, however, could potentially be utilized with any program that docks to a rigid protein structure.

For CDK2, both ligands self-dock and the smaller ligand (CDK2:L1) cross-docks correctly, while the larger ligand (CDK2:L2) does not cross-dock correctly into the protein structure (CDK2:P1) obtained with the smaller ligand bound, as anticipated (Figure 5A and B). The larger ligand, CDK2:L2



**Figure 5.** Superposition of X-ray structures for CDK2 and FXa, respectively, by matching all heavy atoms. The superimposed CDK2:P1-L1 (cyan carbons) and CDK2:P2-L2 (yellow carbons) protein structures are shown in (A) with the CDK2:L1 ligand and in (B) with the CDK2:L2 ligand visible. For clarity the backbone of D86 and the side chains of E81 and L83 are not shown. The superimposed FXa:P1-L1 (white carbons) and FXa:P2-L2 (green carbons) protein structures are shown in (C) with the FXa:L1 ligand and in (D) with the FXa:L2 ligand visible. All residues are from the heavy chain, and for clarity the backbone atoms for residues Y319, F396, D413, and Q416 are not shown. In all figures, hydrogen bonds between the ligand and its corresponding native protein structure are indicated by dashed lines.

**Table 2. Results of Direct Rigid Docking to the X-ray Structures of CDK2 and FXa<sup>c</sup>**

Protein	RMSD <sup>a</sup>	Glide Score <sup>b</sup>	RMSD	Glide Score
CDK2		L1		L2
P1	0.44	-9.91	5.41	-4.65
P2	0.70	-8.80	0.46	-12.11
FXa		L1		L2
P1	1.28	-10.58	2.54	-9.91
P2	8.41	-8.71	0.50	-11.66

<sup>a</sup>RMSD in Å of heavy atoms after superimposing the proteins.

<sup>b</sup>GlideSP score for the top pose from Glide docking. <sup>c</sup>The highlighted regions represent cross-docking results. Green represents a ligand RMSD below 2.0 Å, yellow represents a ligand RMSD between 2.0 and 2.6 Å, and red represents a ligand RMSD above 2.6 Å.

(staurosporine) in its X-ray position, would sterically clash with the backbone of Ile-10, Gly-11, Leu-83 and His-84 as well as the side chain of Gln-131 in the CDK2:P1 protein (Figure 5B; with the closest heavy atom distance 2.0 Å to Leu-83). For FXa, the FXa:L1 and FXa:L2 ligands dock into their native structures correctly, but both fail to cross-dock. The binding mode predicted when docking FXa:L1 into the FXa:P2 protein structure is incorrect with the ligand flipped and partially out of the binding pocket (RMSD 8.41 Å), while that obtained for docking FXa:L2 into the FXa:P1 protein structure is close to correct (RMSD 2.54 Å). FXa:L1, in its X-ray position, would sterically clash with the side chain of H:Tyr-319 in the FXa:P2 protein (Figure 5C; with the closest heavy atom distance 1.4 Å), while FXa:L2 would clash with the H:Gln-416 of the FXa:P1 protein structure (Figure 5D; with the closest heavy atom distance 1.1 Å). These results indicate that for CDK2 and FXa, in general, accurate cross-docking requires that some degree of protein flexibility be taken into account; the softened van der Waals term employed with Glide SP scoring is not sufficient to account for protein flexibility in these cases. It is

also critical that protein flexibility be accounted for in a manner that does not in any way degrade the accuracy obtained when docking to the rigid protein structures; i.e., the ability to self-dock the ligands into ensembles generated from their native protein structures as well as the ability to dock the smaller CDK2 ligand (CDK2:L1) into the ensemble from the protein structure with the somewhat larger binding pocket must be maintained.

With our ensemble-based docking via biased-MD approach, the MD is biased with various restraints to generate ensembles of conformations in an automated manner for docking (Figure 3). For all ensemble-generation protocols, self-docking as well as cross-docking of the CDK2:L1 ligand into the CDK2:P2 protein system serve as controls, since rigid docking is sufficient and gives a correct poses in these cases. The results obtained using the “normal MD” protocol with no restraints on the ligand during the simulation of the complex are shown for CDK2 (Table 3) and FXa (Table 4) and serve as a benchmark.

**Table 3. Docking Results for “normal MD” Generated Ensembles of CDK2**

CDK2	“normal MD” simulations <sup>a,b</sup>			
	RMSD	Glide Score	RMSD	
			L1	L2
P1-L1 Run1	0.67	-10.11	1.72	-10.06
P1-L1 Run2	0.61	-10.84	1.72	-11.33
P1-L1 Run3	1.75	-10.53	1.55	-10.42
P1-L1 Run4	0.96	-10.51	4.67	-7.57
P1-L1 Run5	0.75	-10.63	0.65	-10.59
P2-L2 Run1	0.93	-8.48	0.53	-11.25
P2-L2 Run2	1.12	-8.45	0.85	-11.79
P2-L2 Run3	1.27	-7.98	1.30	-10.81
P2-L2 Run4	0.67	-8.37	1.00	-11.29
P2-L2 Run5	0.86	-8.43	1.11	-11.11

<sup>a</sup>RMSD in Å of the best scoring GlideSP pose after docking to the ensemble, relative to the corresponding X-ray pose. <sup>b</sup>The highlighted regions represent cross-docking results. Green represents a ligand RMSD of below 2.0 Å, yellow represents a ligand RMSD between 2.0 and 2.6 Å, and red represents a ligand RMSD being above 2.6 Å. Noncontrol calculations are shown within thick borders.

With the “normal MD” ensembles, for all of the controls, docking accuracies are maintained, with the exception of self-docking with the FXa:P1-L1 Run4 ensemble which yielded an RMSD of 2.43 Å (a near-native pose). While the “normal MD” ensembles, in general yield correct poses for the control calculations, the RMSDs are somewhat increased relative to those for docking directly to the rigid protein structure. For example, with self-docking to the “normal MD” ensembles for

**Table 4. Docking Results for “normal MD” Generated Ensembles of FXa**

FXa	“normal MD” simulations <sup>a,b</sup>				
	RMSD	Glide Score	RMSD	Glide Score	
	L1		L2		
P1-L1 Run1	1.32	-10.62	2.08	-10.14	
P1-L1 Run2	1.55	-11.27	0.96	-9.82	
P1-L1 Run3	1.37	-11.39	1.89	-10.30	
P1-L1 Run4	2.43	-11.38	1.70	-11.65	
P1-L1 Run5	1.40	-10.42	3.28	-9.70	
P2-L2 Run1	2.06	-9.90	1.14	-10.97	
P2-L2 Run2	1.71	-10.09	0.96	-12.22	
P2-L2 Run3	2.09	-9.89	0.78	-11.50	
P2-L2 Run4	1.58	-10.31	0.95	-11.16	
P2-L2 Run5	1.65	-9.74	0.69	-11.30	

<sup>a</sup>RMSD in Å of the best scoring GlideSP pose after docking to the ensemble, relative to the corresponding X-ray pose. <sup>b</sup>The highlighted regions represent cross-docking results. Green represents a ligand RMSD of below 2.0 Å, yellow represents a ligand RMSD between 2.0 and 2.6 Å, and red represents a ligand RMSD being above 2.6 Å. Noncontrol calculations are shown within thick borders.

CDK2, the RMSDs range from 0.53 to 1.30 Å (for the five distinct ensembles, generated from 5 MD runs) compared to 0.46 Å for docking directly to the rigid X-ray structure. This increase in RMSD reflects the noise introduced into the results by docking to an MD generated ensemble, relative to an experimentally determined protein structure.

Noncontrol cross-docking with the “normal MD” ensembles does not yield consistent results. For CDK2, docking the CDK2:L2 ligand into the ensemble generated from the CDK2:P1-L1 system yields a correct pose for only four out of the five ensembles. Again, these ensembles are all generated using the “normal MD” protocol on the CDK2:P1-L1 system, but using a different random seed to start the MD. For the Run4 ensemble, for which cross-docking failed, the ligand in the correct pose would clash with at least one residue (Ile-10, Gly-11, Leu-83, His-84, or Gln-131) in each of the ensemble protein conformations. For FXa, cross-docking consistently yields correct poses for the FXa:L1 ligand, but not for the FXa:L2. For FXa:L2, a correct pose is obtained for four of the five ensembles. In the one ensemble that fails to yield a correct pose for FXa:L2, all protein conformations would produce a steric clash between the ligand in the correct position and Glu-369 and Gln-416 (Figure 5C and D).

In an attempt to better understand these results, the “normal MD” simulations for both systems were visually inspected. Often during these simulations, the ligand undergoes significant translation relative to its X-ray position within the protein

pocket. In addition, a small degree of flexing of the staurosporine ligand out of plane was observed during its simulations (Figure 6). Diverse (and possibly nonphysically

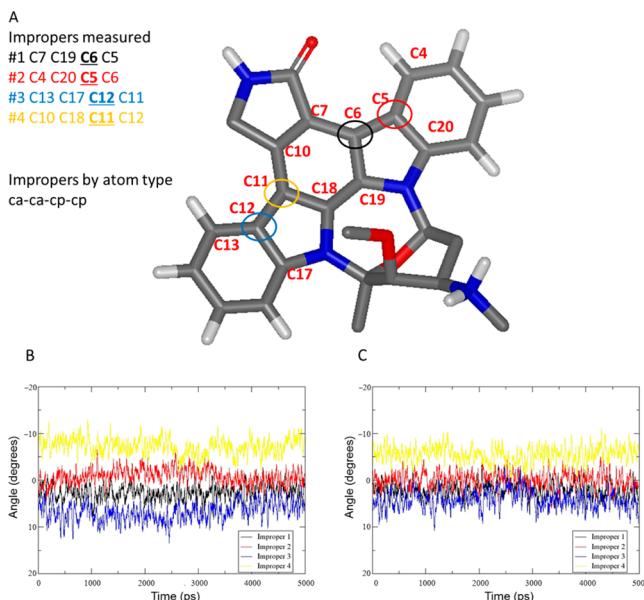


**Figure 6.** Examination of staurosporine (CDK2:L2) impropers as depicted in (A) across MD trajectories that generated the ensembles that ultimately resulted in the best self-docking. Plotted in (B) for the Run 1 normal simulations of CDK2:P2-L2 and in (C) for the Run 2 double improper simulations of CDK2:P2-L2.

relevant) ligand positions and conformations during the simulations used to generate the docking ensembles, may cause the protein pocket to adopt unrealistic conformations for binding, adversely biasing the ensembles generated and ultimately the docking poses obtained. These results led us to investigate different ways of biasing the MD simulations to maintain more of the original pocket-ligand information, while still allowing full flexibility of the binding pocket residues. We explored restraining both the position and conformation of the starting ligand (“restrained MD”) or simply the conformation of the starting ligand (“double impropers MD”) during the MD simulations.

The results of using the “restrained MD” protocol to generate docking ensembles are summarized in Tables 5 and 6 for CDK2 and FXa, respectively. For CDK2 and FXa, the control self-docking accuracy is maintained, although again with somewhat larger RMSDs than for direct rigid docking to the corresponding X-ray protein structures. The control cross-docking of CDK2:L1 into the ensemble generated by CDK2:P2-L2 resulted in only three out of five correct poses. In both failures, the two hinge hydrogen bonds to the backbone of Glu-81 and Leu-83 (present in the CDK2:P1-L1 X-ray structure, Figure 5A) are broken. For the cross-docking of CDK2:L2, a correct pose is obtained for four of the five ensembles (Table 5). For the one failure (RMSD 5.47 Å), the correct binding mode is not obtained due to the position of Gln-131 (Figure 5). This potential clash may be due to inadequate sampling of the conformation of Gln-131 during the CDK2:P1-L1 MD simulation, preventing successful cross-docking of the CDK2:L2 ligand. For FXa cross-docking of FXa:L1 yields a correct pose with four of the five ensembles, and a near native pose (2.57 Å RMSD) with the other

**Table 5. Docking Results for “restrained MD” Generated Ensembles of CDK2**

CDK2	“restrained MD” simulations <sup>a,b</sup>				
	RMSD	Glide Score	RMSD	Glide Score	
	L1		L2		
P1-L1 Run1	0.54	-10.36	1.31	-9.75	
P1-L1 Run2	0.64	-10.04	5.47	-8.29	
P1-L1 Run3	1.03	-10.70	1.15	-9.62	
P1-L1 Run4	0.58	-10.59	1.50	-10.53	
P1-L1 Run5	0.81	-10.45	1.59	-10.52	
P2-L2 Run1	1.62	-8.09	1.28	-10.89	
P2-L2 Run2	5.60	-8.07	0.79	-11.57	
P2-L2 Run3	1.39	-8.39	1.00	-11.05	
P2-L2 Run4	1.51	-8.45	1.44	-10.15	
P2-L2 Run5	5.29	-8.27	0.95	-12.42	

<sup>a</sup>RMSD in Å of the best scoring GlideSP pose after docking to the ensemble, relative to the corresponding X-ray pose. <sup>b</sup>The highlighted regions represent cross-docking results. Green represents a ligand RMSD of below 2.0 Å, yellow represents a ligand RMSD between 2.0 and 2.6 Å, and red represents a ligand RMSD being above 2.6 Å. Noncontrol calculations are shown within thick borders.

**Table 6. Docking Results for “restrained MD” Generated Ensembles of FXa**

FXa	“restrained MD” simulations <sup>a,b</sup>				
	RMSD	Glide Score	RMSD	Glide Score	
	L1		L2		
P1-L1 Run1	1.76	-11.20	2.67	-11.16	
P1-L1 Run2	1.07	-10.91	1.66	-10.66	
P1-L1 Run3	1.42	-11.71	1.31	-9.75	
P1-L1 Run4	1.72	-10.48	1.65	-9.56	
P1-L1 Run5	1.38	-10.63	1.30	-10.36	
P2-L2 Run1	1.70	-10.06	1.61	-11.27	
P2-L2 Run2	1.63	-10.33	1.36	-11.30	
P2-L2 Run3	2.57	-10.06	0.75	-12.44	
P2-L2 Run4	1.92	-10.35	1.14	-11.27	
P2-L2 Run5	1.79	-10.02	1.64	-11.47	

<sup>a</sup>RMSD in Å of the best scoring GlideSP pose after docking to the ensemble, relative to the corresponding X-ray pose. <sup>b</sup>The highlighted regions represent cross-docking results. Green represents a ligand RMSD of below 2.0 Å, yellow represents a ligand RMSD between 2.0 and 2.6 Å, and red represents a ligand RMSD being above 2.6 Å. Noncontrol calculations are shown within thick borders.

ensemble. Cross-docking of FXa:L2 also yields a correct pose with four of the five ensembles (Table 6). The one miss (2.67 Å RMSD) is likely due to the conformations of Gln-416 sampled during the “restrained MD” simulation; Gln-416 in the FXa:P1-L1 X-ray structure would sterically clash with FXa:L2 (Figure 5C). Overall the “restrained MD” ensembles yielded reduced docking accuracies relative to the “normal MD” ensembles. Perhaps the restraints on the ligand position, in addition to its conformation, caused the protein pocket to adopt less relevant conformations overall.

To maintain the experimentally known conformation of the starting ligand during the MD simulations, and sample more extensively around the original pocket-ligand conformation, we employed the “double impropers MD” protocol for generating the docking ensembles. For CDK2 (Table 7) and FXa (Table 8), the control docking accuracy is fully maintained, although as anticipated with larger RMSDs than for direct rigid docking. Furthermore, noncontrol cross-docking for both CDK2 and FXa more consistently yields a correct pose as the top ranked pose. For CDK2:L2 and FXa:L1 cross-docking, respectively, one of the five ensembles generated yields a near native pose, while all other ensembles yield correct poses with RMSDs less than 2 Å relative to the corresponding X-ray structure. Even the near native poses, if they were the only ones obtained, would be expected to be suitable for use in structure-based drug design (see Figure 7).

The “double impropers MD” are able to produce ensembles that yield the most consistently accurate docking results. RMSD plots (Figure 8) comparing the binding pocket residues at various points in the simulations to the starting structures, suggest that the “double impropers MD” simulations better maintain the overall pocket conformation (while allowing for specific side chain movements as indicated in Figure 7) throughout the simulation, to ultimately generate ensembles that produce better docking results. Comparing RMSD plots for the “double impropers MD” vs the “normal MD” simulations (as in Figure 8) also helps to quantify the differences in “noise” between the different simulation protocols. Doubling of the ligand improper terms clearly better maintains the bound starting ligand conformation, for staurosporine in this example, during the MD simulations (Figure 6) leading to enhanced docking results overall. Biasing the MD simulations in this manner likely retains more relevant pocket-ligand information, that is ultimately reflected in more accurate ensemble-based docking. In addition, and perhaps equally importantly, this work shows that with protein flexibility taken into account in this way, the Glide SP docking is able to identify consistently a correct pose as the top pose. It remains to be seen if the addition of a solvation correction in a postprocessing step could further improve docking accuracy.

**Table 7. Docking Results for “double impropers MD” Generated Ensembles of CDK2**

CDK2	“double impropers MD” simulations <sup>a,b</sup>				
	RMSD	Glide Score	RMSD	Glide Score	
	L1		L2		
P1-L1 Run1	0.66	-10.31	2.55	-10.61	
P1-L1 Run2	0.82	-10.93	1.95	-8.84	
P1-L1 Run3	1.28	-10.80	1.68	-7.94	
P1-L1 Run4	0.76	-10.14	1.80	-9.85	
P1-L1 Run5	0.60	-11.48	1.27	-10.03	
P2-L2 Run1	1.85	-8.36	1.70	-10.26	
P2-L2 Run2	1.38	-7.74	0.61	-10.73	
P2-L2 Run3	2.01	-8.07	1.52	-10.28	
P2-L2 Run4	1.09	-8.10	0.88	-10.42	
P2-L2 Run5	1.30	-8.13	1.02	-10.80	

<sup>a</sup>RMSD in Å of the best scoring GlideSP pose after docking to the ensemble, relative to the corresponding X-ray pose. <sup>b</sup>The highlighted regions represent cross-docking results. Green represents a ligand RMSD of below 2.0 Å, yellow represents a ligand RMSD between 2.0 and 2.6 Å, and red represents a ligand RMSD being above 2.6 Å. Noncontrol calculations are shown within thick borders.

## CONCLUSIONS

From a modeling standpoint, arguably one of the most important components is the bridge between computation and experimental “reality”. Often the starting point for an MD simulation is an X-ray protein–ligand complex structure, which may be partial or complete in terms of the protein chains, and sometimes the ligand is a substrate. During the simulation, the structure inevitably drifts away from the starting point due to thermal fluctuations. In this work, to generate the docking ensemble, we limit the drift that occurs during the MD simulation by adding an additional biasing potential to retain the starting ligand conformation and thereby maintain the binding pocket near a state that is known to be relevant, the crystallographic one. In the subsequent, ensemble-based docking the new ligands are successfully docked, fully flexibly, to rigid protein conformations represented in the ensemble.

In drug discovery, the overall goal of any docking scheme is to provide the most accurate predictions possible in a time frame fast enough to have impact on the optimization project. With the ensemble-based approach described in this manuscript, there is an upfront cost. At the beginning of a given drug discovery project, an ensemble must be created from an existing protein–ligand structure. For our test cases, typical MD runs took 45–48 CPU hours on 8 cores at 2.93 GHz with an Intel Xeon x5670 processor and 24 GB of memory. While significant, this compute time is not unreasonable since it is a one-time cost. Also, with the use of GPU computing it is possible that a

**Table 8. Docking Results for “double impropers MD” Generated Ensembles of FXa**

FXa	“double impropers MD” simulations <sup>a,b</sup>				
	RMSD	Glide Score	RMSD	Glide Score	
	L1		L2		
P1-L1 Run1	1.83	-11.19	1.22	-8.92	
P1-L1 Run2	1.49	-12.00	1.45	-11.86	
P1-L1 Run3	1.43	-10.68	1.80	-11.26	
P1-L1 Run4	1.74	-10.12	0.84	-9.93	
P1-L1 Run5	1.22	-11.10	1.39	-10.55	
P2-L2 Run1	1.66	-10.49	1.09	-11.53	
P2-L2 Run2	1.52	-10.55	0.58	-11.65	
P2-L2 Run3	1.83	-9.77	1.50	-11.62	
P2-L2 Run4	1.49	-9.71	1.02	-12.64	
P2-L2 Run5	2.41	-10.93	2.38	-12.09	

<sup>a</sup>RMSD in Å of the best scoring GlideSP pose after docking to the ensemble, relative to the corresponding X-ray pose. <sup>b</sup>The highlighted regions represent cross-docking results. Green represents a ligand RMSD of below 2.0 Å, yellow represents a ligand RMSD between 2.0 and 2.6 Å, and red represents a ligand RMSD being above 2.6 Å. Noncontrol calculations are shown within thick borders.

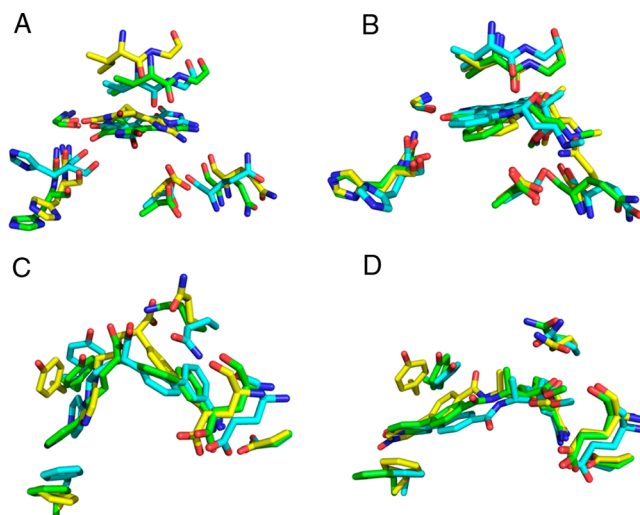


**Figure 7.** Superposition of X-ray structure (cyan carbons) and corresponding top poses for cross-docking to of (A) CDK2:L1 into the CDK2:P2-L2 generated ensemble, (B) CDK2:L2 into the CDK2:P1-L1 generated ensemble, (C) FXa:L1 into the FXa:P2-L2 generated ensemble, and (D) FXa:L2 into the FXa:P1-L1 generated ensemble. For each, the best (green carbons) and worst (yellow carbons) “top pose” from Tables 7 and 8, respectively, based on RMSD, are shown to indicate the spread in the top poses obtained.

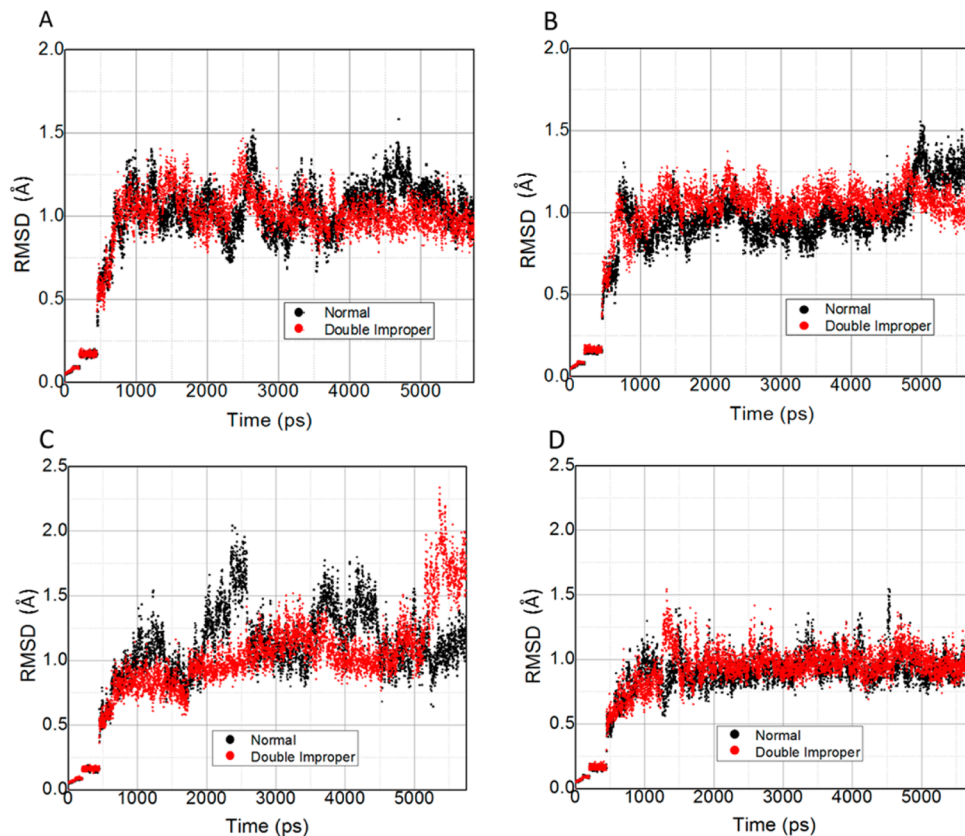


**Figure 8.** RMSD plots comparing the binding pocket residues at points across the MD trajectory to the starting structure, for MD simulations that generated ensembles that ultimately resulted in the worst and best cross-docking results, respectively. For CDK2:P1-L1, in (A) for normal simulations (Run 4, worst) and double improper simulations (Run 1, worst), and in (B) for normal simulations (Run 5, best) and double improper simulations (Run 5, best). For FXa:P1-L1, in (C) for normal simulations (Run 5, worst) and double improper simulations (Run 3, worst), and in (D) for normal simulations (Run 2, best) and double improper simulations (Run 4, best).

30- to 100-fold speedup may be realized. After creation of an ensemble, all project ligands (existing and proposed) can be docked to that ensemble. At that point, the required CPU time per ligand is simply the docking time of the program being employed (in this case Glide SP) times the number of protein conformations in the ensemble (eight times approximately 4/s/ligand).

In summary, a novel ensemble-based docking approach using biased-MD simulation is presented. The approach is unique in that the sampling of binding pocket conformations is enhanced by applying a biasing potential to maintain the bound conformation of the ligand from the original protein–ligand complex structure. In this way, sufficient sampling is achieved, while reducing the introduction of noise through the generation of irrelevant pocket conformations for binding, ultimately resulting in more consistently accurate docking results. While this approach may not be applicable to larger domain motions, we believe ensemble-based docking via biased-MD method represents an advanced, practical approach in the structure-based design drug discovery tool box.

## ■ ASSOCIATED CONTENT

### ● Supporting Information

Ligand parameters are given in Tables S1–S4. This material is available free of charge via the Internet at <http://pubs.acs.org>.

## ■ AUTHOR INFORMATION

### Corresponding Author

\*E-mail: diane.j-m@enbiotix.com.

### Present Address

<sup>†</sup>EnBiotix, Inc. 197 W. Springfield St., Boston, MA 02118.

### Notes

The authors declare no competing financial interest.

## ■ ACKNOWLEDGMENTS

The authors would like to thank Sameer Kawatkar for many helpful discussions and review of the manuscript.

## ■ REFERENCES

- (1) Munos, B. Lessons from 60 years of pharmaceutical innovation. *Nat. Rev. Drug Discovery* **2009**, *8*, 959–968.
- (2) Nichols, S. E.; Baron, R.; Ivetac, A.; McCammon, J. A. Predictive power of molecular dynamics receptor structures in virtual screening. *J. Chem. Inf. Model.* **2011**, *51*, 1439–1446.
- (3) McCammon, J. A.; Gelin, B. R.; Karplus, M. Dynamics of folded proteins. *Nature* **1977**, *267*, 585–590.
- (4) Adcock, S. A.; McCammon, J. A. Molecular dynamics: survey of methods for simulating the activity of proteins. *Chem. Rev.* **2006**, *106*, 1589–1615.
- (5) McMartin, C.; Bohacek, R. S. QXP: powerful, rapid computer algorithms for structure-based drug design. *J. Comput.-Aided Mol. Des.* **1997**, *11*, 333–344.
- (6) Hornak, V.; Abel, R.; Okur, A.; Strockbine, B.; Roitberg, A.; Simmerling, C. Comparison of multiple Amber force fields and

- development of improved protein backbone parameters. *Proteins* **2006**, *65*, 712–725.
- (7) Case, D. A.; Darden, T. A.; Cheatham, T. E., III; Simmerling, C. L.; Wang, J.; Duke, R. E.; Luo, R.; Walker, R. C.; Zhang, W.; Merz, K. M.; Roberts, B. P.; Wang, B.; Hayik, S.; Roitberg, A.; Seabra, G.; Kolossváry, I.; Wong, K. F.; Paesani, F.; Vanicek, J.; Liu, J.; Wu, X.; Brozell, S. R.; Steinbrecher, T.; Gohlke, H.; Cai, Q.; Ye, X.; Wang, J.; Hsieh, M.-.; Cui, G.; Roe, D. R.; Mathews, D. H.; Seetin, M. G.; Sagui, C.; Babin, V.; Luchko, T.; Gusarov, S.; Kovalenko, A.; Kollman, P. A. *AMBER 11*; University of California, San Francisco, CA, 2010.
- (8) Bowers, K. J.; Chow, E.; Xu, H.; Dror, R. O.; Eastwood, M. P.; Gregersen, B. A.; Klepeis, J. L.; Kolossváry, I.; Moraes, M. A.; Sacerdoti, F. D.; Salmon, J. K.; Shan, Y.; Shaw, D. E. In *Scalable Algorithms for Molecular Dynamics Simulations on Commodity Clusters*. Proceedings from the ACM/IEEE Conference on Supercomputing (SC06), Tampa, Florida, November 11–17, 2006; IEEE: New York, 2006.
- (9) Phillips, J. C.; Braun, R.; Wang, W.; Gumbart, J.; Tajkhorshid, E.; Villa, E.; Chipot, C.; Skeel, R. D.; Kale, L.; Schulten, K. Scalable molecular dynamics with NAMD. *J. Comput. Chem.* **2005**, *26*, 1781–1802.
- (10) Shaw, D. E.; Deneroff, M. M.; Dror, R. O.; Kuskin, J. S.; Larson, R. H.; Salmon, J. K.; Young, C.; Batson, B.; Bowers, K. J.; Chao, J. C.; Eastwood, M. P.; Gagliardo, J.; Grossman, J. P.; Ho, C. R.; Ierardi, D. J.; Kolossváry, I.; Klepeis, J. L.; Layman, T.; McLeavy, C.; Moraes, M. A.; Mueller, R.; Priest, E. C.; Shan, Y.; Spengler, J.; Theobald, M.; Towles, B.; Wang, S. C. Anton, a special-purpose machine for molecular dynamics simulation. *Commun. ACM* **2008**, *S1*, 91–97.
- (11) Shan, Y.; Kim, E. T.; Eastwood, M. P.; Dror, R. O.; Seeliger, M. A.; Shaw, D. E. How does a drug molecule find its target binding site? *J. Am. Chem. Soc.* **2011**, *133*, 9181–9183.
- (12) Amaro, R. E.; Li, W. W. Emerging methods for ensemble-based virtual screening. *Curr. Top. Med. Chem.* **2010**, *10*, 3–13.
- (13) Nichols, S. E.; Baron, R.; McCammon, J. A. On the use of molecular dynamics receptor conformations for virtual screening. *Methods Mol. Biol.* **2012**, *819*, 93–103.
- (14) Craig, I. R.; Essex, J. W.; Spiegel, K. Ensemble docking into multiple crystallographically derived protein structures: an evaluation based on the statistical analysis of enrichments. *J. Chem. Inf. Model.* **2010**, *50*, 511–524.
- (15) Rueda, M.; Bottegoni, G.; Abagyan, R. Recipes for the selection of experimental protein conformations for virtual screening. *J. Chem. Inf. Model.* **2010**, *50*, 186–193.
- (16) Bottegoni, G.; Rocchia, W.; Rueda, M.; Abagyan, R.; Cavalli, A. Systematic exploitation of multiple receptor conformations for virtual ligand screening. *PLoS One* **2011**, *6*, e18845.
- (17) Sherman, W.; Day, T.; Jacobson, M. P.; Friesner, R. A.; Farid, R. Novel procedure for modeling ligand/receptor induced fit effects. *J. Med. Chem.* **2006**, *49*, 534–553.
- (18) Amaro, R. E.; Baron, R.; McCammon, J. A. An improved relaxed complex scheme for receptor flexibility in computer-aided drug design. *J. Comput.-Aided Mol. Des.* **2008**, *22*, 693–705.
- (19) Schames, J. R.; Henchman, R. H.; Siegel, J. S.; Sotriffer, C. A.; Ni, H.; McCammon, J. A. Discovery of a novel binding trench in HIV integrase. *J. Med. Chem.* **2004**, *47*, 1879–1881.
- (20) Cavasotto, C. N.; Abagyan, R. A. Protein flexibility in ligand docking and virtual screening to protein kinases. *J. Mol. Biol.* **2004**, *337*, 209–225.
- (21) Carlson, H. A.; Masukawa, K. M.; Rubins, K.; Bushman, F. D.; Jorgensen, W. L.; Lins, R. D.; Briggs, J. M.; McCammon, J. A. Developing a dynamic pharmacophore model for HIV-1 integrase. *J. Med. Chem.* **2000**, *43*, 2100–2114.
- (22) Robustelli, P.; Kohlhoff, K.; Cavalli, A.; Vendruscolo, M. Using NMR chemical shifts as structural restraints in molecular dynamics simulations of proteins. *Structure* **2010**, *18*, 923–933.
- (23) Isin, B.; Schulten, K.; Tajkhorshid, E.; Bahar, I. Mechanism of signal propagation upon retinal isomerization: insights from molecular dynamics simulations of rhodopsin restrained by normal modes. *Bioophys. J.* **2008**, *95*, 789–803.
- (24) Gerek, Z. N.; Ozkan, S. B. A flexible docking scheme to explore the binding selectivity of PDZ domains. *Protein Sci.* **2010**, *19*, 914–928.
- (25) Cavasotto, C. N.; Kovacs, J. A.; Abagyan, R. A. Representing receptor flexibility in ligand docking through relevant normal modes. *J. Am. Chem. Soc.* **2005**, *127*, 9632–9640.
- (26) Rueda, M.; Totrov, M.; Abagyan, R. ALIBERO: evolving a team of complementary pocket conformations rather than a single leader. *J. Chem. Inf. Model.* **2012**, *52*, 2705–2714.
- (27) Venkatraman, V.; Ritchie, D. W. Flexible protein docking refinement using pose-dependent normal mode analysis. *Proteins* **2012**, *80*, 2262–2274.
- (28) Schulze-Gahmen, U.; De Bondt, H. L.; Kim, S. H. High-resolution crystal structures of human cyclin-dependent kinase 2 with and without ATP: bound waters and natural ligand as guides for inhibitor design. *J. Med. Chem.* **1996**, *39*, 4540–4546.
- (29) Davie, E. W.; Fujikawa, K.; Kisiel, W. The coagulation cascade: initiation, maintenance, and regulation. *Biochemistry* **1991**, *30*, 10363–10370.
- (30) Borensztajn, K.; Spek, C. A. Blood coagulation factor Xa as an emerging drug target. *Expert Opin. Ther. Targets* **2011**, *15*, 341–349.
- (31) Kamata, K.; Kawamoto, H.; Honma, T.; Iwama, T.; Kim, S. H. Structural basis for chemical inhibition of human blood coagulation factor Xa. *Proc. Natl. Acad. Sci. U. S. A.* **1998**, *95*, 6630–6635.
- (32) Guertin, K. R.; Gardner, C. J.; Klein, S. I.; Zulli, A. L.; Czekaj, M.; Gong, Y.; Spada, A. P.; Cheney, D. L.; Maignan, S.; Guilloteau, J. P.; Brown, K. D.; Colussi, D. J.; Chu, V.; Heran, C. L.; Morgan, S. R.; Bentley, R. G.; Dunwiddie, C. T.; Leadley, R. J.; Pauls, H. W. Optimization of the beta-aminoester class of factor Xa inhibitors. Part 2: Identification of FXV673 as a potent and selective inhibitor with excellent *In vivo* anticoagulant activity. *Bioorg. Med. Chem. Lett.* **2002**, *12*, 1671–1674.
- (33) Hamdouchi, C.; Zhong, B.; Mendoza, J.; Collins, E.; Jaramillo, C.; De Diego, J. E.; Robertson, D.; Spencer, C. D.; Anderson, B. D.; Watkins, S. A.; Zhang, F.; Brooks, H. B. Structure-based design of a new class of highly selective aminoimidazo[1,2-a]pyridine-based inhibitors of cyclin dependent kinases. *Bioorg. Med. Chem. Lett.* **2005**, *15*, 1943–1947.
- (34) Jakalian, A.; Bush, B. L.; Jack, D. B.; Bayly, C. I. Fast, efficient generation of high-quality atomic charges. AM1-BCC model: I. Method. *J. Comput. Chem.* **2000**, *21*, 132–146.
- (35) Jakalian, A.; Jack, D. B.; Bayly, C. I. Fast, efficient generation of high-quality atomic charges. AM1-BCC model: II. Parameterization and validation. *J. Comput. Chem.* **2002**, *23*, 1623–1641.
- (36) Wang, J.; Wolf, R. M.; Caldwell, J. W.; Kollman, P. A.; Case, D. A. Development and testing of a general amber force field. *J. Comput. Chem.* **2004**, *25*, 1157–1174.
- (37) Bradbrook, G. M.; Gleichmann, T.; Harrop, S. J.; Habash, J.; Raftery, J.; Kalb, J.; Yariv, J.; Hillier, I. H.; Helliwell, J. R. X-Ray and molecular dynamics studies of concanavalin-A glucoside and mannose complexes Relating structure to thermodynamics of binding. *J. Chem. Soc., Faraday Trans.* **1998**, 1603–1611.
- (38) Jorgensen, W. L.; Chandrasekhar, J.; Madura, J. D.; Impey, R. W.; Klein, M. L. Comparison of simple potential functions for simulating liquid water. *J. Chem. Phys.* **1983**, *79*, 926–935.
- (39) Darden, T.; York, D.; Pedersen, L. Particle mesh Ewald: An  $N \log(N)$  method for Ewald sums in large systems. *J. Chem. Phys.* **1993**, *98*, 10089–10092.
- (40) Cheatham, T. E., III; Miller, J. L.; Fox, T.; Darden, T. A.; Kollman, P. A. Molecular Dynamics Simulations on Solvated Biomolecular Systems: The Particle Mesh Ewald Method Leads to Stable Trajectories of DNA, RNA, and Proteins. *J. Am. Chem. Soc.* **1995**, *117*, 4193–4194.
- (41) Ryckaert, J.; Ciccotti, G.; Berendsen, H. J. C. Numerical integration of the cartesian equations of motion of a system with constraints: molecular dynamics of n-alkanes. *J. Comput. Phys.* **1977**, *23*, 327–341.

- (42) Shao, J.; Tanner, S. W.; Thompson, N.; Cheatham, T. E. Clustering Molecular Dynamics Trajectories: 1. Characterizing the Performance of Different Clustering Algorithms. *J. Chem. Theory Comput.* **2007**, *3*, 2312–2334.
- (43) Verdonk, M. L.; Mortenson, P. N.; Hall, R. J.; Hartshorn, M. J.; Murray, C. W. Protein-ligand docking against non-native protein conformers. *J. Chem. Inf. Model.* **2008**, *48*, 2214–2225.
- (44) Friesner, R. A.; Banks, J. L.; Murphy, R. B.; Halgren, T. A.; Klicic, J. J.; Mainz, D. T.; Repasky, M. P.; Knoll, E. H.; Shelley, M.; Perry, J. K.; Shaw, D. E.; Francis, P.; Shenkin, P. S. Glide: a new approach for rapid, accurate docking and scoring. 1. Method and assessment of docking accuracy. *J. Med. Chem.* **2004**, *47*, 1739–1749.
- (45) Halgren, T. A.; Murphy, R. B.; Friesner, R. A.; Beard, H. S.; Frye, L. L.; Pollard, W. T.; Banks, J. L. Glide: a new approach for rapid, accurate docking and scoring. 2. Enrichment factors in database screening. *J. Med. Chem.* **2004**, *47*, 1750–1759.
- (46) Koska, J.; Spassov, V. Z.; Maynard, A. J.; Yan, L.; Austin, N.; Flook, P. K.; Venkatachalam, C. M. Fully automated molecular mechanics based induced fit protein-ligand docking method. *J. Chem. Inf. Model.* **2008**, *48*, 1965–1973.
- (47) Warren, G. M.; McGaughey, G. B.; Nevins, N. Editorial. *J. Comput.-Aided Mol. Des.* **2012**, *26*, 674.
- (48) Repasky, M. P.; Murphy, R. B.; Banks, J. L.; Greenwood, J. R.; Tubert-Brohman, I.; Bhat, S.; Friesner, R. A. Docking performance of the glide program as evaluated on the Astex and DUD datasets: a complete set of glide SP results and selected results for a new scoring function integrating WaterMap and glide. *J. Comput.-Aided Mol. Des.* **2012**, *26*, 787–799.
- (49) Cheng, T.; Li, X.; Li, Y.; Liu, Z.; Wang, R. Comparative assessment of scoring functions on a diverse test set. *J. Chem. Inf. Model.* **2009**, *49*, 1079–1093.
- (50) Warren, G. L.; Andrews, C. W.; Capelli, A. M.; Clarke, B.; LaLonde, J.; Lambert, M. H.; Lindvall, M.; Nevins, N.; Semus, S. F.; Senger, S.; Tedesco, G.; Wall, I. D.; Woolven, J. M.; Peishoff, C. E.; Head, M. S. A critical assessment of docking programs and scoring functions. *J. Med. Chem.* **2006**, *49*, 5912–5931.
- (51) Wang, R.; Lu, Y.; Wang, S. Comparative evaluation of 11 scoring functions for molecular docking. *J. Med. Chem.* **2003**, *46*, 2287–2303.